POLITECNICO DI TORINO
Repository ISTITUZIONALE

Fast hardware protection for a series-series compensated inductive power transfer system for electric vehicles

Original
Fast hardware protection for a series-series compensated inductive power transfer system for electric vehicles / Ganga, A.L., Cirimele, V., Ruffo, R., Guglielmi, P.. - ELETTRONICO. - (2017), pp. 1-6. (2017 IEEE Southern Power Electronics Conference (SPEC) Puerto Varas, Chile 4-7 Dec. 2017) [10.1109/SPEC.2017.8333626].

Availability:
This version is available at: 11583/2705475 since: 2018-04-10T11:06:39Z

Publisher:
IEEE

Published
DOI:10.1109/SPEC.2017.8333626

Terms of use:

This article is made available under terms and conditions as specified in the corresponding bibliographic description in the repository

Publisher copyright
IEEE postprint/Author's Accepted Manuscript

©2017 IEEE. Personal use of this material is permitted. Permission from IEEE must be obtained for all other uses, in any current or future media, including reprinting/republishing this material for advertising or promotional purposes, creating new collecting works, for resale or lists, or reuse of any copyrighted component of this work in other works.

(Article begins on next page)

13 October 2026

Fast Hardware Protection for a Series-Series Compensated Inductive Power Transfer System for Electric Vehicles

Alessandro La Ganga, Vincenzo Cirimele, Riccardo Ruffo, Paolo Guglielmi

Politecnico di Torino, Department of Energy,
Corso Duca degli Abruzzi 24, 10129, Torino, Italy
emails: name.surname@polito.it

***Abstract*—The paper proposes a simple solution to a safety problem encountered during the development of a series-series compensated IPT system for electric vehicles. This problem is related to the equivalent current source behavior of the receiver side in presence of an unpredicted load disconnection. A pure analog hardware system able to manage this fault protecting the filtering elements of the system is proposed. The system is investigated by means of a circuit simulation then its physical implementation is presented. The effectiveness of the proposed solution is experimentally proven.**

***Index Terms*—Power system protection, inductive power transfer (IPT).**

I. Introduction

Despite the limitations still presented by batteries, the market of electric vehicles (EVs) is continuously growing and car manufactures are producing new electric models. This change, in the view of private and public transportation, is forcing the creation of an electrical infrastructure for the charge of electric vehicles. At the same time, this is introducing the need for safer and easy to use charging systems that can be installed in the urban environment without demanding high maintenance costs and the necessity of strong modifications in the existent infrastructure.

In EVs context, the wireless charging systems are encountering a continuously growing interest. In particular, the development of a series of market-ready products based on the inductive power transfer (IPT) is ongoing. This process is accompanied by the creation of a series of international standards [1].

IPT is based on the inductive coupling of a coil fixed on or under the ground level, named transmitter, and a second coil placed under the vehicle floor called receiver. The transmitter is powered through a power electronics (PE) converter providing a high-frequency current that gives rise to a high-frequency magnetic field. This magnetic field links with the receiver allowing the transfer of electrical power. By means of the connection of a rectification stage, the transferred power can be used to charge the EV battery. Thanks to the absence of electrical contacts, the two parts of the system can be independently enclosed, the transmitter can be placed directly under the ground pavement eliminating the necessity of external installations.

A generic scheme of an IPT system for EVs is depicted in Fig. 1. The impedances of both transmitter and receiver coils are compensated by introducing capacitive elements that can be directly connected in series or in parallel or by creating more complex network of reactive elements [2]–[5]. The compensation is mandatory to maximize the power transfer capability of the system reducing at the same time the VA rating and then the cost of the source [6].

The present paper focuses on a hardware protection system developed for a series-series compensated system supplied by a VSI converter. The presented solution has come from a direct experience in the development of an IPT system able to transfer up to 11 kW to the vehicle battery. As it is better detailed in the next sections, the developed protection circuit has stemmed from the need to protect the power electronics and the capacitive filters on the receiver side against unpredicted sudden disconnections of the load. However, the presented results can be applied to other system architectures.

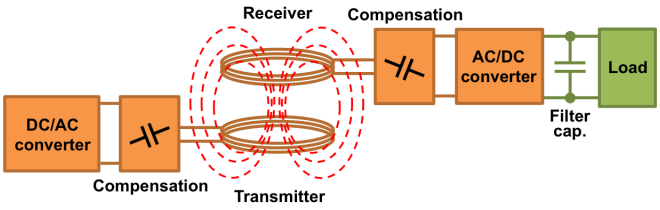

Fig. 1. General scheme of an IPT system.

II. System model and equations

The IPT system sketched in Fig. 1 can be represented through the simplified circuit model of Fig. 2 where L_1 and L_2 are the self-inductances of transmitter and receiver respectively and M is the mutual inductance between them. The source is modeled by means of a sinusoidal voltage source representing the first harmonic of the voltage at the output of the DC/AC converter that powers the system. This PE stage is generally based on an H-bridge architecture [3], [7]–[9]. In several

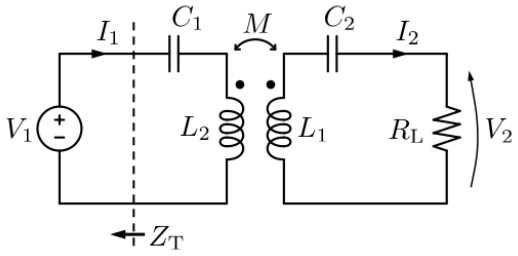

Fig. 2. Circuit model of the series-series compensated IPT system.

applications, the rectification stage is constituted by a diode bridge connected to the battery by means of a capacitive filter [3], [7], [10]. In some cases, a synchronous rectifier or a chain of a diode bridge and a DC/DC converter is also proposed [8], [11], [12]. In each case, this stage can be conveniently modeled through an equivalent resistive load R_L representing the ratio of the first harmonic of voltage and current at the AC/DC converter input. The two capacitors C_1 and C_2 are connected in series with the respective coil on the base of the relation

$$\omega_0 = \frac{1}{\sqrt{L_1 C_1}} = \frac{1}{\sqrt{L_2 C_2}} \tag{1}$$

where ω_0 is the global resonant frequency of the system i.e. the working frequency of the source. In this case the resistances of coils and capacitors are not considered as this approximation does not affect the analysis and the derived results.

The entire IPT system can be described, at the source terminals, by the total impedance $\bar{Z}_\mathrm{T}$. This impedance, is equal to the ratio of the first harmonic of voltage and current at the DC/AC converter output and it is defined as:

$$\bar{Z}_\mathrm{T} = \frac{\overline{V}_1}{\overline{I}_1} = \mathrm{j}\left(\omega L_1 - \frac{1}{\omega C_1}\right) + \frac{\omega^2 M^2}{R_\mathrm{L} + \mathrm{j}\left(\omega L_2 - \frac{1}{\omega C_2}\right)} \tag{2}$$

At the resonance, i.e. $\omega = \omega_0$, the coils and capacitors impedances compensate each other and the total impedance presents only a real component expressed as:

$$Z_T = \frac{\omega^2 M^2}{R_\mathrm{L}} \tag{3}$$

The voltage V_1 and the current I_1 are then in phase, so it is possible to express the transmitter current as:

$$I_1 = \frac{R_\mathrm{L}}{\omega^2 M^2} V_1 \tag{4}$$

The current I_1 gives rise to an induced voltage V_oc in the receiver defined as:

$$V_\mathrm{oc} = \omega M I_1 \tag{5}$$

This voltage is called open-circuit voltage as it can be measured at the receiver terminals when no load is connected. At the resonance, V_oc is directly applied to the load, hence the induced current in the receiver can by expressed as:

$$I_2 = \frac{V_\mathrm{oc}}{R_\mathrm{L}} = \frac{\omega_0 M}{R_\mathrm{L}} I_1 \tag{6}$$

By substituting (4) into (6) it is possible to rewrite the receiver current as:

$$I_2 = \frac{V_1}{\omega_0 M} \tag{7}$$

This last equation shows that, for a certain voltage V_1, the current I_2 is independent of the load. This means that the receiver part behaves like a current source. This behavior can be extremely dangerous in case of a fault that leads to a sudden disconnection of the load. In fact, also if the load is disconnected from the output of the DC/DC converter, the current I_2 would continue to flow in the filter capacitor at the AC/DC converter output. This causes an abrupt increase of the capacitor voltage that can lead to the dielectric break down of the component with consequent risks of explosion.

As will be detailed in Section IV, the rapidity of this fault event cannot be managed by a current control on the transmitter side. It is worth noting that, from (3), the absence of the load results in an equivalent short circuit behavior of the total impedance that can lead to an increase of the current I_1.

The carried out analysis demonstrates that, the fast dynamic introduced by an eventual load disconnection fault, has to be already carefully taken into account during the design of the system. The intervention of the protection must be as fast as the filter capacitor voltage rate of rise so an analog hardware system has been considered to be the most suited solution.

III. Fast hardware protection

The scheme of the protection circuit is shown in Fig. 3. It is inserted close to the component that have to be protected (i.e. the filter capacitor C_f) between the AC/DC converter and the load. The same position would be used also in presence of an additional DC/DC converter that interfaces with the load. In this way all the components downstream of the DC/DC converter are intrinsically protected.

The role of the protection circuit is to intervene by short-circuiting the receiver once the voltage over the capacitor C_f exceeds a certain safety threshold. The short circuit is a compatible condition with respect to the current source behavior of the receiver. At the same time, as can be noticed from (3), the short circuit of the receiver leads to an open circuit behavior of the equivalent impedance that forces the current I_1 to zero. In this way, the fault and the intervention of the protection can be easily detected at the transmitter side without the need for communication between the two sides of the IPT system.

The protection circuit is based on three Zener diodes D_{z1}, D_{z2} and D_{z3} and the thyristor T. The Zener diodes are chosen in order to obtain an overall breakdown voltage equal to the maximum allowable voltage over the capacitor. This voltage level is chosen to be compatible also with the load (e.g. maximum tolerable voltage of the EV battery). If the voltage over the capacitor exceeds the total breakdown threshold, the Zener diodes start to conduct giving rise to the activation of the thyristor that short-circuits the receiver. This short circuit

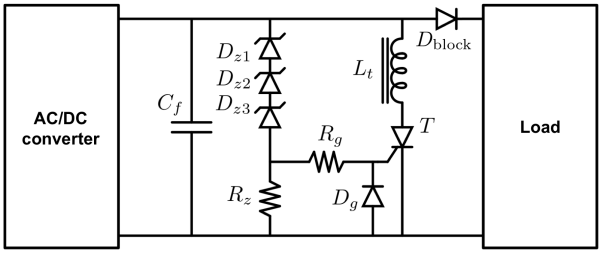

Fig. 3. Scheme of the protection system and its connection in the IPT system.

causes the discharge of the filter capacitor whose voltage is lowered.

Additional components are introduced to guarantee a compatible and safe intervention of the protection circuit. The resistor R_z is placed in the Zener diodes branch in order to limit the current when the diodes start to operate in the breakdown region. Similarly, the resistor R_g is used to limit the current that can flow in the thyristor gate to a compatible level. The diode D_g, connected between the thyristor gate and the cathode, is placed to avoid possible inversion of the polarity of the gate voltage that can be due to the resonance of the circuit parasitics stimulated during the thyristor transition.

As the intervention of the protection circuit consists in an abrupt discontinuity in the capacitor voltage, this component reacts by injecting a current pulse in the thyristor. While the peak of this current pulse has to be limited to protect the capacitor, the rate of rise of this current has to be limited in order to avoid the break of the thyristor. This issue is faced through the insertion of the inductor L_t whose role is to limit the time derivative of the current to a value compatible with the thyristor characteristics.

Finally, the diode D_{block} is necessary if a battery is directly connected as load. When the short circuit is carried out, this diode avoids the inversion of the battery current towards the receiver coil.

IV. Simulation

The effectiveness of the proposed solution has been preliminary tested by means of a circuit simulation using a SPICE software. As shown in Fig. 4, the simulation has been performed taking into account both sides of the IPT system. The values of the system parameters and the values of the considered components for the simulation of the protection circuit are reported in Table I.

In the tested prototype, the AC/DC converter is constituted of a diode bridge. The capacitive filter consists of the parallel of three capacitors C_{f1}, C_{f2} and C_{f3} whose equivalent series resistance (ESR) and inductance (ESL) have been modeled. The Zener diodes and the thyristor have been modeled by adapting already available SPICE models. The overall threshold voltage of the diodes has been set to 450 V. The load has been simply modeled with a resistance whose disconnection is carried out by a time dependent switch that turns off once the system reaches the steady-state. The transmitter side is supplied by a square wave voltage source. The value of the inductance L_t has been chosen in order to limit the time derivative of the current to a value of 250 A$/\mu$s in correspondence to an applied step voltage equal to the overall breakdown voltage of the diodes. For the sake of simplicity, possible phenomena of saturation of the inductor core have been neglected then L_t has been treated by using a linear model. Despite this simplification, the effectiveness of the current derivative limitation resulting from the simulation can be considered valid for the first instants following the turn on of the thyristor. Once the turn on transition is completed, this limitation is less stringent so a non linearity of the inductor does not lead to problems of compatibility.

TABLE I
VALUES OF THE PARAMETERS FOR THE SIMULATION OF IPT SYSTEM AND PROTECTION CIRCUIT

Parameters	**Symbol**	**Value**
Working frequency	f_0	85 kHz
Amplitude of the source voltage	V_{pk}	500 V
Rms value of the source voltage	V_1	450 V
Rated voltage at the diode bridge output	V_{DC}	300 V
Rated transmitter current	I_1	28.5 A
Rated receiver current	I_2	50 A
Rated total impedance	Z_{T}	15.8 Ω
Equivalent load resistance	R_{Load}	4 Ω
Transmitter self-inductance	L_1	281 μH
Receiver self-inductance	L_2	120 μH
Nominal mutual inductance	M	14.3 μH
Transmitter resistance	R_1	0.78 Ω
Receiver resistance	R_2	0.53 Ω
Transmitter capacitor	C_1	12.5 nF
Receiver capacitor	C_2	29.2 nF
Single filter capacitor	C_{f}	3 μF
Single filter capacitor ESL	L_{f}	48 nF
Single filter capacitor ESR	R_{f}	2.8 mΩ
Current limiter inductor	L_{t}	1.8 μH
Gate resistor	R_{g}	10 Ω
Zener diodes series resistor	R_{z}	100 Ω
Zener diodes overall breakdown voltage	V_{z}	450 V

The results of the simulation are shown in Fig. 5. The load is disconnected after 1 ms of simulation. At this time the system reached the steady-state condition then the capacitor is charged at its rated value $V_{\text{DC}} = 300$ V. After the load disconnection, the filter capacitor voltage starts to immediately increase with a rate of rise of 7 V$/\mu$s while the transmitter current I_1 remains practically unvaried in the first instants. This justifies the modeling of the source by not considering the presence of an active control of the current. In other words, the dynamic of the transient on the receiver is faster than the related dynamic in the transmitter and the fault can not be promptly recognized from the source side. When the voltage V_{DC} reaches the threshold voltage of the Zener diodes, the activation of the thyristor occurs forcing the short circuit of the capacitor. The forced discharge of the capacitor gives rise to a high current peak of about 1000 A with a rate of rise of about 250 A$/\mu$s limited by the inductor L_t. The current peak is reached 8 μs after the thyristor turn on then the current tends towards the value of the current at the diode bridge output in the pre-fault conditions. It is worth noting

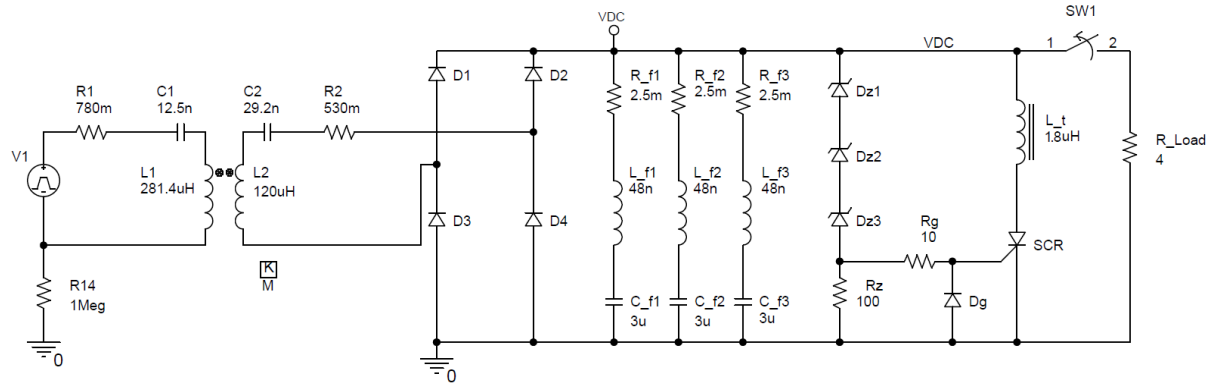

Fig. 4. Scheme of the circuit for the SPICE simulation.

that, even if the current reaches a value of several hundreds of amperes, its energetic content is limited to about one joule (i.e. the energy stored in the capacitor before the protection circuit intervention) so it can be transiently managed by the PE switches without introducing thermal problems.

As visible in Fig. 5(b), the short circuit of the receiver forces the current in the transmitter towards zero via a series of sinusoidal pulsations. This behavior is typical of the magnetically coupled resonant circuit [13] but is not here treated in detail.

V. Implementation and Testing

The ensemble of diode bridge, filter capacitors and protection circuit has been implemented and mounted in a unique compact case that has been directly connected to the receiver coil and the compensating capacitor. The resulting object is shown in Fig. 6 and Fig. 7 while the adopted components for the protection circuit are listed in Table II.

Table II
Adopted components for the protection circuit

Components	Symbol	Model
Zener diode	D_{z1}	1N5368B
Zener diodes	D_{z2}, D_{z3}	1N5388B
Thyristor	T	MCO150-12io1
Filter capacitors	C_{f1}, C_{f2}, C_{f3}	C4BSPBX4300Z

All the components have been chosen by considering a safety factor of two with respect to the values obtained from the simulation. The chosen thyristor is able to carry a rated current of 158 A with a maximum forward surge current of 2 kA. The same component can tolerate a non repetitive current time derivative of 500 A/μs. The overall threshold voltage of 450 V has been obtained by combining two Zener diodes 1N5388B with a breakdown threshold of 200 V in series with the Zener diode 1N5368B having a breakdown threshold of 50 V. The filter capacitors have rated voltage and current of 630 V and 38 A respectively. Each capacitor can tolerate a repetitive current peak of 1793 A. The inductor L_t has been built by using two C-shaped cores made of laminated silicon steel.

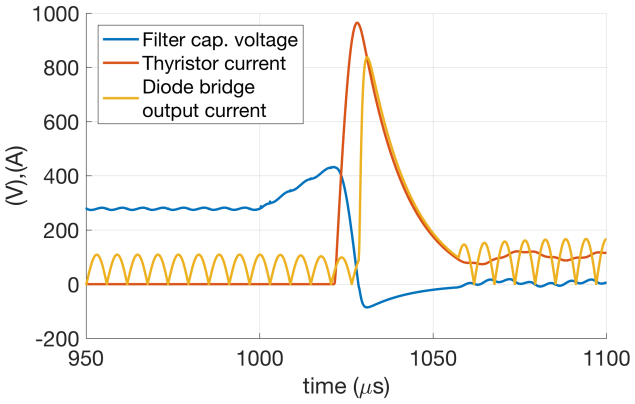

(a)

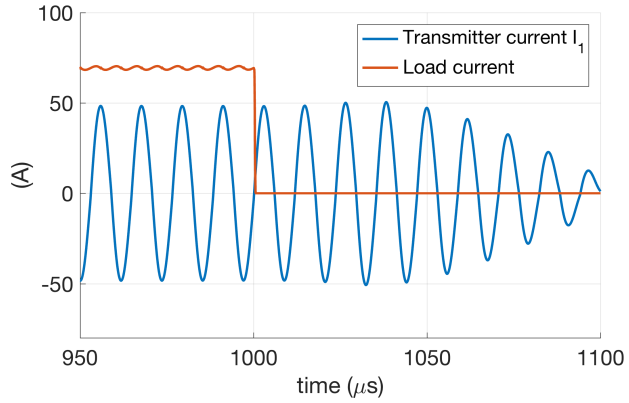

(b)

Fig. 5. Representative waveforms of the SPICE simulation of the protection circuit intervention. (a) Voltage V_{DC} over the capacitors C_{f1}, C_{f2} and C_{f3} and current in the thyristor L_t. (b) Transmitter current I_1 and load current.

The system has been tested by directly supplying the diode bridge with an isolated voltage supply. The output voltage of the supply has been varied via ramp until reaching the overall breakdown voltage of the Zener diodes. This has allowed a slow charge of the filter capacitor while maintaining controlled the current provided by the supply.

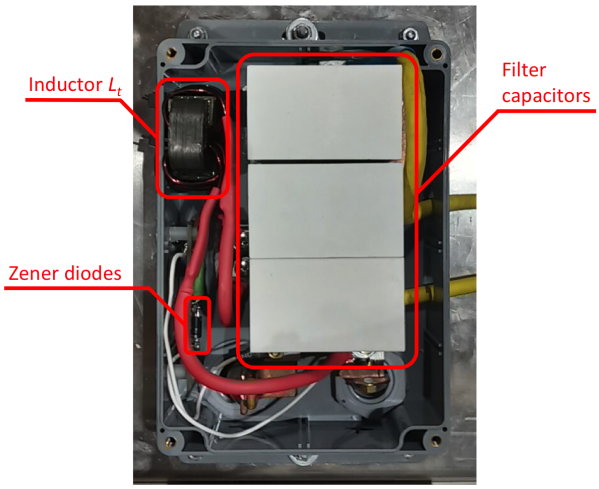

Fig. 6. Top view of the implemented system mounted on the receiver side. The box contains the diode bridge converter, the filter capacitors and protection circuitry.

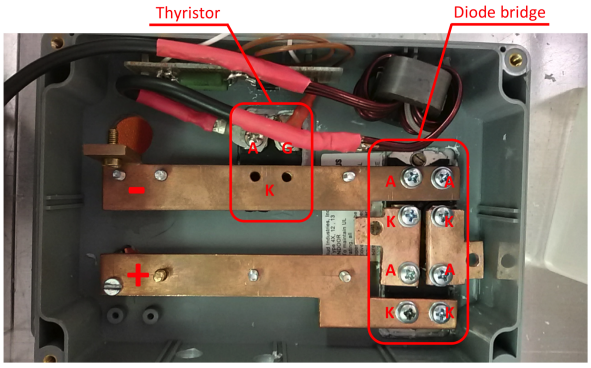

Fig. 7. Top view of the implemented system where the filter capacitors are not mounted. The bus bar structure is visible together with the mounting positions of the thyristor T and the diode bridge.

The measured waveforms during the protection circuit intervention are shown in Fig. 8. The current in the thyristor branch has been measured by using a Rogowski probe having an output scale of $0.2\ \mathrm{mV/A}$. The intervention of the protection circuit occurs for a voltage of $480\ \mathrm{V}$ slightly higher than the ideally desired threshold but perfectly compatible with the maximum tolerable voltage of the filter capacitors. The thyristor turn on is carried out correctly and the current time derivative remains under the critical rate of rise of the thyristor. Contrary to what observed in simulation, several oscillation phenomena appear. These phenomena are linked to the connections parasitics not taken into account in the simulation model together with the interaction of the protection circuit with the reactive elements of the voltage supply. In particular the observed oscillations of the thyristor gate voltage are due to the selection of the measurement points. As the thyristor cathode was not directly accessible, the measurements have been carried out between the thyristor anode and the pin of the resistor R_z connected to the negative of the DC bus.

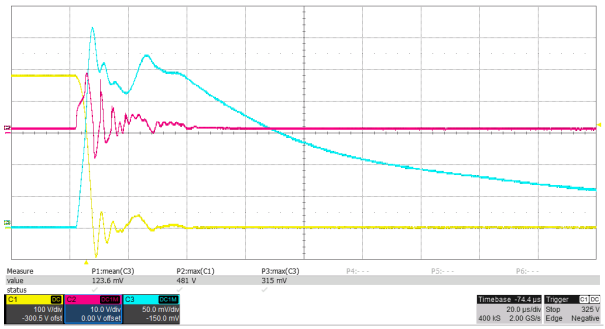

Fig. 8. Measured waveforms of the tested protection circuit intervention. Filter capacitor voltage V_{DC} in yellow ($100\ \mathrm{V/div}$). Gate voltage of the thyristor in magenta ($10\ \mathrm{V/div}$). Current in the thyristor branch in cyan ($50\ \mathrm{mV/div}$ corresponding to $250\ \mathrm{A/div}$).

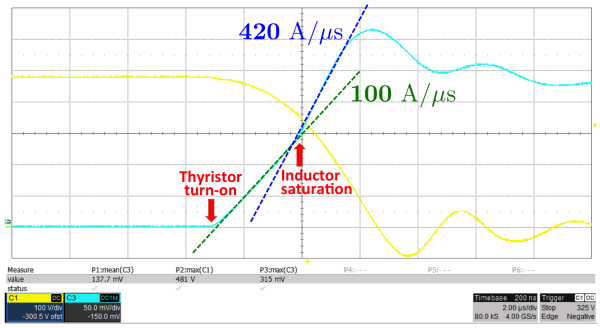

Fig. 9. Measured waveforms of the tested protection circuit intervention. Filter capacitor voltage V_{DC} in yellow ($100\ \mathrm{V/div}$). Current in the thyristor branch in cyan ($50\ \mathrm{mV/div}$ corresponding to $250\ \mathrm{A/div}$).

Fig. 9 shows in detail the behavior of the voltage over the filter capacitors and the current in the thyristor branch. The change in the current slope clearly indicates the saturation of the inductance core. The saturation occurs once the thyristor is turned on then the increased time derivative of the current does not represent a problem. Because of the saturation, the current peak reaches a higher value than the one observed in simulation but it remains below the tolerated values of thyristor and capacitors.

As expected, the current peak is perfectly managed by the thyristor and the diodes. Finally, the testing of the system demonstrates its effectiveness.

VI. Conclusions

The paper has described a safety problem encountered during direct experience in the development of an IPT systems for the charge electric vehicles. The model and the analytical expressions used to describe the origin of the problem have been based on a series-series compensated system supplied by means of a VSI converter. However, the same conclusions can be considered valid for other kinds of system topologies for which the receiver behaves like a current source. For these systems the disconnection of the load is not compatible and can represent a dangerous conditions for the capacitive components connected to the rectification stage. The fast

dynamic introduced by the load disconnection fault has needed the development of an analog hardware protection circuit. This protection circuit has been studied and designed with the help of a circuit simulation and its effectiveness has been experimentally proven.

VII. Acknowledgment

This work has been co-funded by the European Unions 7th Framework Program for Research, namely through the FABRIC project under grant agreement no. 605405.

References

[1] V. Cirimele, F. Freschi, and M. Mitolo, "Inductive power transfer for automotive applications: State-of-the-art and future trends," in *2016 IEEE Industry Applications Society Annual Meeting*, Oct 2016, pp. 1–8.

[2] Del Toro García, Xavier and Vázquez, Javier and Roncero-Sánchez, Pedro, "Design, implementation issues and performance of an inductive power transfer system for electric vehicle chargers with series–series compensation," *IET Power Electronics*, vol. 8, no. 10, pp. 1920–1930, 2015.

[3] J. Huh, S. W. Lee, W. Y. Lee, G. H. Cho, and C. T. Rim, "Narrow-Width Inductive Power Transfer System for Online Electrical Vehicles," *IEEE Transactions on Power Electronics*, vol. 26, no. 12, pp. 3666–3679, Dec 2011.

[4] W. Li, H. Zhao, S. Li, J. Deng, T. Kan, and C. C. Mi, "Integrated LCC Compensation Topology for Wireless Charger in Electric and Plug-in Electric Vehicles," *IEEE Transactions on Industrial Electronics*, vol. 62, no. 7, pp. 4215–4225, July 2015.

[5] S. Zhou and C. C. Mi, "Multi-Paralleled LCC Reactive Power Compensation Networks and Their Tuning Method for Electric Vehicle Dynamic Wireless Charging," *IEEE Transactions on Industrial Electronics*, vol. 63, no. 10, pp. 6546–6556, Oct 2016.

[6] C.-S. Wang, G. A. Covic, and O. H. Stielau, "Power transfer capability and bifurcation phenomena of loosely coupled inductive power transfer systems," *IEEE Transactions on Industrial Electronics*, vol. 51, no. 1, pp. 148–157, Feb 2004.

[7] O. C. Onar, J. M. Miller, S. L. Campbell, C. Coomer, C. P. White, and L. E. Seiber, "A novel wireless power transfer for in-motion ev/phev charging," in *Applied Power Electronics Conference and Exposition (APEC), 2013 Twenty-Eighth Annual IEEE*. IEEE, 2013, pp. 3073–3080.

[8] U. K. Madawala, M. Neath, and D. J. Thrimawithana, "A Power-Frequency Controller for Bidirectional Inductive Power Transfer Systems," *IEEE Transactions on Industrial Electronics*, vol. 60, no. 1, pp. 310–317, Jan 2013.

[9] S. G. Rosu, M. Khalilian, V. Cirimele, and P. Guglielmi, "A dynamic wireless charging system for electric vehicles based on DC/AC converters with SiC MOSFET-IGBT switches and resonant gate-drive," in *IECON 2016 - 42nd Annual Conference of the IEEE Industrial Electronics Society*, Oct 2016, pp. 4465–4470.

[10] A. Pevere, R. Petrella, C. C. Mi, and S. Zhou, "Design of a high efficiency 22 kW wireless power transfer system for EVs fast contactless charging stations," in *Electric Vehicle Conference (IEVC), 2014 IEEE International*. IEEE, 2014, pp. 1–7.

[11] J. L. Villa, J. Sallán, A. Llombart, and J. F. Sanz, "Design of a high frequency inductively coupled power transfer system for electric vehicle battery charge," *Applied Energy*, vol. 86, no. 3, pp. 355–363, 2009.

[12] U. K. Madawala and D. J. Thrimawithana, "Current sourced bi-directional inductive power transfer system," *IET Power Electronics*, vol. 4, no. 4, pp. 471–480, April 2011.

[13] X. Ju, L. Dong, X. Huang, and X. Liao, "Switching Technique for Inductive Power Transfer at High- Q Regimes," *IEEE Transactions on Industrial Electronics*, vol. 62, no. 4, pp. 2164–2173, April 2015.